

Article

Effect of Sn Content in a CuSnZn Metal Precursor on Formation of MoSe₂ Film during Selenization in Se+SnSe Vapor

Liyong Yao¹, Jianping Ao^{1,*}, Ming-Jer Jeng^{2,*}, Jinlian Bi¹, Shoushuai Gao¹, Guozhong Sun¹, Qing He¹, Zhiqiang Zhou¹, Yun Sun¹ and Liann-Be Chang²

¹ Institute of Photoelectronic Thin Film Devices and Technology and Tianjin Key Laboratory of Thin film Devices and Technology, Nankai University, Tianjin 300071, China; yaoliyong@yeah.net (L.Y.); bijinlian815@126.com (J.B.); gaoshoushuai@yeah.net (S.G.); taigic@nankai.edu.cn (G.S.); Heqing27@nankai.edu.cn (Q.H.); zhqzhou@126.com (Z.Z.); suny@nankai.edu.cn (Y.S.)

² Department of Electronic Engineering, Chang Gung University, Taoyuan City 33302, Taiwan; liann@mail.cgu.edu.tw

* Correspondence: aojp@nankai.edu.cn (J.A.); mjeng@mail.cgu.edu.tw (M.-J.J.); Tel.: +86-22-2350-8572 (ext. 8011) (J.A.); +886-3-211-8800 (ext. 3507) (M.-J.J.); Fax: +86-22-2350-2778 (J.A.); +886-3-211-8507 (M.-J.J.)

Academic Editor: Christof Schneider

Received: 14 January 2016; Accepted: 22 March 2016; Published: 29 March 2016

Abstract: The preparation of Cu₂ZnSnSe₄ (CZTSe) thin films by the selenization of an electrodeposited copper–tin–zinc (CuSnZn) precursor with various Sn contents in low-pressure Se+SnSe_x vapor was studied. Scanning electron microscope (SEM) and energy dispersive spectroscopy (EDS) measurements revealed that the Sn content of the precursor that is used in selenization in a low-pressure Se+SnSe_x vapor atmosphere only slightly affects the elemental composition of the formed CZTSe films. However, the Sn content of the precursor significantly affects the grain size and surface morphology of CZTSe films. A metal precursor with a very Sn-poor composition produces CZTSe films with large grains and a rough surface, while a metal precursor with a very Sn-rich composition procures CZTSe films with small grains and a compact surface. X-ray diffraction (XRD) and SEM revealed that the metal precursor with a Sn-rich composition can grow a thicker MoSe₂ thin film at CZTSe/Mo interface than one with a Sn-poor composition, possibly because excess Sn in the precursor may catalyze the formation of MoSe₂ thin film. A CZTSe solar cell with an efficiency of 7.94% was realized by using an electrodeposited metal precursor with a Sn/Cu ratio of 0.5 in selenization in a low-pressure Se+SnSe_x vapor.

Keywords: Cu₂ZnSnSe₄ solar cells; selenization; electrodeposited CuSnZn precursor; MoSe₂; Se+SnSe_x vapor

1. Introduction

Earth-abundant and non-toxic light absorber materials, such as Cu₂ZnSn(S_xSe_{1-x})₄ (CZTSSe), are attractive for use in the Tera-Watt scale production of thin film solar cells that have adjustable bandgaps of between 1.0 to 1.5 eV and a theoretical efficiency of 30% [1–12]. These materials are still in an incipient state of development, and the Cu₂ZnSnSe₄ (CZTSe) and CZTSSe solar cells have a maximum device efficiency of 11.6% [4] and 12.6% [5], respectively. The selenization of metal precursors has been demonstrated to be a promising method for large-area and high-efficiency CZTSe solar cells [11,12]. A precursor, wholly [4,5,10] or partially [11–14] with CZTSe, was first prepared via vacuum or non-vacuum method and then was selenized by thermal treatment to improve its crystallinity. An inert gas and selenium (Se) at high partial pressures are commonly used to

ensure the surface stability at the expense of the diffusion of excess Se diffusing through CZTSe thin films, which then reacts with molybdenum (Mo) to form thick molybdenum diselenide (MoSe_2) films [15]. These thick MoSe_2 films detrimentally affect high-efficiency CZTSe solar cells. Reducing the formation of MoSe_2 films is a matter of great interest. Severe tin (Sn) loss is commonly observed during high-temperature selenization in the preparation of CZTSe films [16–18]. This critical problem arises mainly from the decomposition of CZTSe films. Excess Sn in the precursor is commonly compensates the loss of Sn [19]. However, a thick MoSe_2 film at CZTSe/Mo interface is observed following the selenization of the metal precursor that contains excess Sn [13]. Shin [15], and Scragg [20] studied the mechanism of formation of the MoSe_2 film. A high Se concentration in the selenization atmosphere causes Se to diffuse through the CZTSe thin film and react with Mo to form a MoSe_2 film. However, the mechanism of formation is used only with a near-stoichiometric composition [3,21]. The effect of the Sn content of the precursor on the formation of MoSe_2 films has not yet been studied. This study investigates CZTSe films that are prepared by the selenization of the metal precursor with various Sn contents in low-pressure Se+SnSe vapor atmospheres, with a focus on the relationship between the Sn content and the formation of MoSe_2 films.

2. Experimental Section

Electrodeposited thin metal stacks were used to fabricate CZTSe thin films by selenization. The cathode in the electrodeposition process was a 4 cm × 4 cm piece of soda-lime glass on which a 1200-nm-thick double molybdenum (Mo) layer was deposited by DC magnetron sputtering. Before the Mo thin films were deposited, the substrates were ultrasonically cleaned in a detergent bath, followed by acetone, isopropanol, and DI water. The DC power was then set at 450 W at room temperature during sputtering. Next, Mo bilayer films were deposited to obtain good adhesion and low resistivity. Mo film was first deposited in a high working pressure of 1.5 Pa for 13 min to obtain good adhesion and then in a low working pressure of 0.1 Pa for 39 min to obtain a low resistivity. The metal stacks of copper (Cu), tin (Sn), and zinc (Zn) were electrodeposited on a Mo layer by the constant current method using a three-electrode system at room temperature. The stacking sequence of the three metals was copper-tin-zinc (CuSnZn) with the Cu layer at the bottom and adjacent to the Mo layer, the Sn layer in the middle, and the zinc layer on the top surface. Table 1 presents the elemental contents of electrodeposited CuSnZn precursors. The ratio of Zn to Cu in electrodeposited CuSnZn precursors was fixed at approximately 0.7. The three ratios of the amount of Sn to the amount of Cu in the electrodeposited CuSnZn precursors were 0.25, 0.5, and 0.75; the corresponding samples were named as A1, A2, and A3, respectively. The proportions of Cu, Sn, and Zn were controlled by adjusting the electroplating times of copper, tin, and zinc. The reference electrode and anode were electrically linked to each other. Copper was electrodeposited from a laboratory-made solution and contained 187.5 g/L of sulfate pentahydrate. Tin was electrodeposited from a commercially available electrodeposition bath, which contained mesylate, tin methanesulfonate, and additives RX-851 from Rongxing Electronics (Zhejiang, China). The solution of zinc was developed in-house using 0.2 M zinc vitriol that was dissolved in 0.5 M methane sulfuric acid. The pH of the solution was adjusted to 2.0 by adding sodium hydroxide. The copper, tin, and zinc layers were electrodeposited using a direct current with current densities of 50, 3, and 20 mA/cm², respectively. The typical deposition time was approximately 100 s.

Table 1. The elemental contents of electrodeposited CuSnZn precursors.

Sample	Cu (%)	Zn (%)	Sn (%)	Zn/Cu	Sn/Cu	Cu/(Zn+Sn)	Zn/Sn
A1	51.28	35.9	12.82	0.70	0.25	1.05	2.80
A2	45.45	31.81	22.74	0.70	0.50	0.83	1.40
A3	40.82	28.57	30.61	0.70	0.75	0.69	0.93

The electrodeposited metal stacks were annealed at 300 °C for 30 min in inert gas at 1000 Pa to ensure the uniform distribution of Cu, Sn, and Zn; they then underwent the selenization processes, as

presented in Figure 1. Samples of the metallic precursors were reactively selenized in a laboratory-made furnace (not a tubular furnace) capable of working in vacuum (10^{-4} Pa) or an inert gas (Ar) atmosphere [22]. The sample temperature, Sn temperature and the Se temperature are controlled individually. The temperature of Sn, Se, and sample were at 550, 270, and 570 °C, respectively. The partial pressure of Se and SnSe_x vapors was approximately 16 and 19 Pa, respectively. The elemental Sn and Se are placed in the selenization furnace, under heating, and Se evaporates into the selenization furnace and reacts with Sn to form SnSe_x binary phases, which evaporates easily due to a high saturated vapor pressure. A standard procedure, without any etching process, was applied to fabricate a CZTSe solar cell with a Mo/CZTSe/CdS/i-ZnO/Al-ZnO/Ni-Al structure. First, a 50-nm-thick CdS was deposited by chemical bath deposition. Next, 50 nm i-ZnO and 450 nm Al-ZnO were deposited by RF sputtering. Finally, a 50-nm Ni/0.2- μ m Al metal grid was deposited on top of the device via electron-beam evaporation through a metal mask to create a metallic grid pattern. The active area of CZTSe solar cell is 0.34 cm².

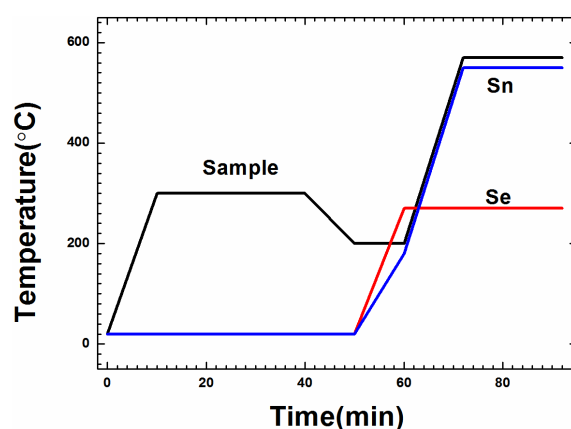


Figure 1. The temperature profiles of the selenization process.

The composition of the CZTSe thin film was obtained using a Magix (PW2403 (PANalytical LTD., EA Almelo, The Netherlands)) X-ray fluorescent spectrometer (XRF) with a Rh-anode, which was calibrated by inductively coupled plasma spectroscopy (ICP). The structures of the samples were characterized by using a Philips X-pert Pro diffractometer (PANalytical Ltd.) with Cu K α radiation and a Renishaw in Via Raman spectroscopy (Renishaw Ltd., Gloucestershire, UK) with an excitation wavelength of 514 nm. The penetration depth of this laser wavelength is around 100 nm into the absorber [23]. Surface and cross-sectional observations were made using a scanning electron microscope with energy dispersive spectroscopy (EDS) analysis. (SEM, JEOL JSM-6700 (JEOL Ltd., Akishima-shi, Japan)). The depth profiles of the elements were obtained by line scanning EDS and secondary ion mass spectroscopy (SIMS) measurements (IMS-4F, CAMAECA, Nancy, France). The incident electron probe size used in EDS measurement was 10 nm (full-width-at-half-maximum). The surface roughness was determined by using an Ambios Technology XP-2 Surface Profiler. Current-voltage (J-V) measurements of CZTSe solar cells were made under illumination by a standard AM1.5 spectrum of 1000W/m² at room temperature with a constant-light solar simulator, which was calibrated using a standard mono-crystalline Si solar cell.

3. Results and Discussion

Figure 2 present the XRD patterns of the electrodeposited CuSnZn precursor before and after annealing at 300 °C for 30 min, respectively. The XRD spectra in Figure 2a included strong Cu, Sn, and Zn elemental peaks and a weak Cu₅Zn₈ alloy peak. Annealing eliminated the Cu, Sn, and Zn elemental peaks and caused the appearance of strong peaks that were associated with Cu₅Zn₈ and Cu₆Sn₅ alloys in Figure 2b. High-temperature annealing promoted the interdiffusion of elements to

form a binary alloy in the metallic stack precursor. The adhesion between CZTSe and Mo was a critical problem in the selenization of the metal precursor in the preparation of CZTSe thin films. Stacked metal layer, especially with the Cu at the bottom, cause bad adhesion between CZTSe films and Mo substrates. The volume of the copper clearly varies during the selenization process, owing to the large disparities between the volume of Cu₂Se and CuSe₂ per one copper atom [24]. The bottom Cu may generate holes at the back contact interface and thereby form many point defects during selenization, detrimentally affecting device performance [14]. After annealing, the formation of the binary alloy in the metallic stack precursor may reduce the number of pin holes and defects formed. Formation of alloy in the precursor favors follow-up selenization for the preparation of high-quality CZTSe films.

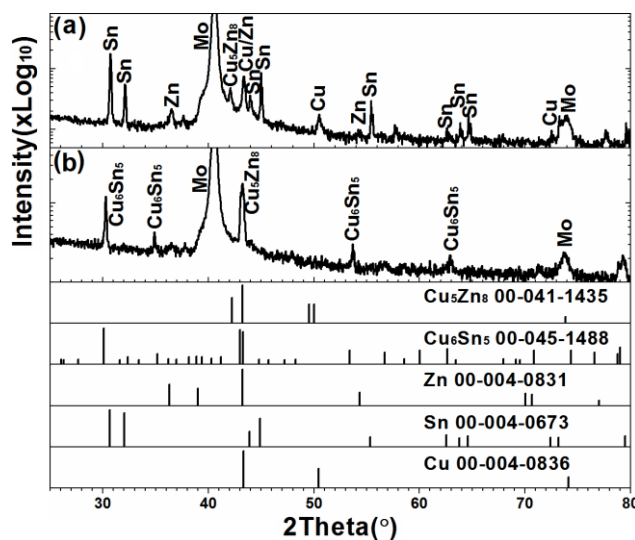


Figure 2. The X-ray diffraction (XRD) patterns of the electrodeposited CuSnZn precursor (a) before; and (b) after annealing at 300 °C for 30 min.

Table 2 presents the elemental contents of the CZTSe films that were prepared by the selenization of the precursor with samples A1, A2, and A3 in a SnSe_x+Se vapor atmosphere. The metal ratio of Zn to Cu in all three samples after selenization is 0.69. As is well known, the Zn has a high saturated vapor pressure at temperatures of over 400 °C [25]. However, during selenization, Zn easily reacts with Se to form a ZnSe compound, which has a low saturated vapor pressure. Therefore, the Zn does not easily evaporate during selenization. Interestingly, the ratio of Sn to Cu varies only slightly between 0.62 and 0.65, even as the Sn/Cu ratio in the precursor is greatly increased from 0.25 to 0.75. A large change in the Sn content of the metal precursor after selenization results in a small change in the Sn content of the formed CZTSe films, mainly owing to the following chemical reaction [16–18].

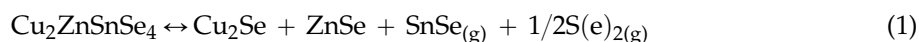


Table 2. The elemental contents of the CZTSe films that were prepared by the selenization of the precursor with samples A1, A2, and A3 in a SnSe_x+Se vapor atmosphere.

Sample	Cu (%)	Zn (%)	Sn (%)	Se(%)	Zn/Cu	Sn/Cu	Cu/(Zn+Sn)	Zn/Sn
A1	21.38	14.75	13.24	50.63	0.69	0.62	0.76	1.11
A2	21.02	14.51	13.19	51.28	0.69	0.63	0.76	1.10
A3	19.86	13.74	12.98	53.42	0.69	0.65	0.74	1.06

The reaction will proceed toward CZTSe (turn to the left reaction) when the Se partial pressure is very high, especially when accompanied by a high inert gas pressure. However, the decomposition

reaction of CZTSe thin films (turn to the right reaction) will occur when the Se partial pressure or inert gas pressure is not high enough. In addition, The CZTSe thin film is stable when SnSe and Se coexist in the selenization atmosphere, which has been confirmed by experiments [17,18]. In Table 2, a large change in the Sn content of the metal precursor after selenization results in a small change in the Sn content of the formed CZTSe films, implying that the reaction is a self-regulating process during the selenization in SnSe and Se atmosphere. When the metal precursor is Sn-rich, the right-hand side of the above chemical reaction (turn to the right reaction) is favored and the excess Sn evaporates off as $\text{SnSe}_{(g)}$. In contrast, when the metal precursor is Sn-poor, the left-hand side of the chemical reaction (turn to the left reaction) is favored and the $\text{SnSe}_{x(g)}$ in the atmosphere reacts with the Se-related containing phases Cu_2Se , ZnSe , and Se to form CZTSe film. Therefore, selenization only slightly changes the Sn content, as presented in Table 2. Similar results have been obtained elsewhere [18].

Figure 3 presents the Raman spectra of the CZTSe films that were prepared by the selenization of the precursor with samples A1, A2, and A3. Peaks at 168, 192, 232, and 244 cm^{-1} , associated with the CZTSe phase, were obtained from all three samples. The Raman patterns of the three samples are very similar, indicating that the surface phases of these CZTSe films were similar because the penetration depth of Raman measurement is around 100 nm into the absorber [23]. The similarity of the phase structures of the three samples arises mainly from the use of a single selenization atmosphere of $\text{Se}+\text{SnSe}_x$ vapor. According to the chemical reaction (1), the same reactive selenization atmosphere will result in the same CZTSe phases. The lack of any MoSe_2 -related peaks from any of the three samples does not reveal the absence of MoSe_2 because the Raman measurements could only be made to a depth of approximately 100 nm with an exciting laser having a wavelength of 514 nm, whereas the thickness of CZTSe films was approximately 2 μm . Therefore, Raman measurement could not detect MoSe_2 films at CZTSe/Mo interface. Accordingly, other measurements, such as XRD or SIMS, had to be made to identify the formation of MoSe_2 .

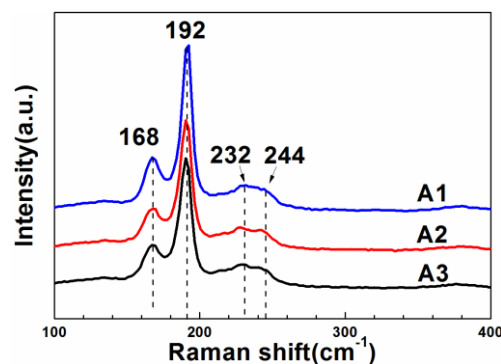


Figure 3. The Raman spectra of the CZTSe films that were prepared by the selenization of the precursor with samples A1, A2, and A3.

Figure 4 presents the XRD spectra of the CZTSe thin films that were prepared by the selenization of the precursor with samples A1, A2, and A3. The CZTSe phases are identified by standard XRD pattern (JCPDS 00-052-0868), based on experimental data. Additional CZTSe diffraction peaks, labeled as * (calculated to correspond to a body-centered tetragonal structure of lattice constants $a = 5.693 \text{ \AA}$ and $c = 11.333 \text{ \AA}$) are also identified. The XRD patterns of the three samples are similar, revealing that they have similar structures. However, sample 3 yielded two strong peaks at 31.6° and 55.9° , which correspond to MoSe_2 structures, indicating that the selenization of metal precursor with excess Sn content may promote the formation of a MoSe_2 layer at the CZTSe/Mo interface. The CZTSe (112) peak position of sample A1, A2, and A3 was 27.14° , 27.17° , and 27.27° , respectively. However, the FWHM of the CZTSe (112) peak was the same value of 0.1299 for the three samples. It cannot observe any difference of grain size from the XRD results of the three samples. According to the standard XRD peaks of CZTSe (00-052-0868) and ZnSe (00-037-1436), the ZnSe (111) peak position has a larger angle

than the CZTSe (112) peak position, implying that the ZnSe secondary phases in the three samples may be different.

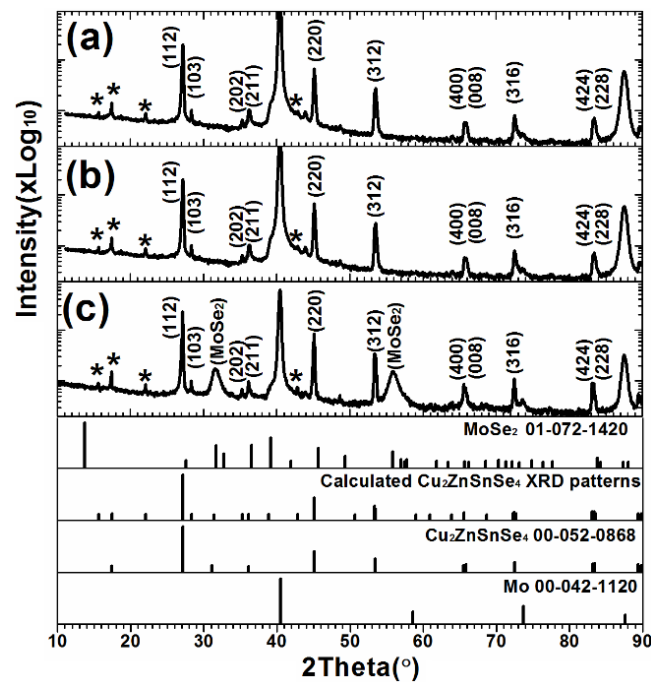


Figure 4. The XRD spectra of the CZTSe thin films that were prepared by the selenization of the precursor with samples (a) A1; (b) A2; and (c) A3.

To confirm the formation of a MoSe₂ thin film at CZTSe/Mo interface, Figure 5 presents the surface morphology and cross-sectional SEM images of the CZTSe films that were prepared by the selenization of the precursor with samples A1, A2, and A3. No MoSe₂ layers are observed in Figure 5a,b. However, the MoSe₂ film is hardly recognizable in Figure 5c. The magnification SEM image of Figure 5c is shown in Figure 6. A clear MoSe₂ layer was observed, consistent with the XRD observation in Figure 4c. The MoSe₂ thin film formed at the CZTSe/Mo interface when the metal precursor contained excess Sn. The SnSe-containing phase (SnSe₂) may have catalyzed the formation of MoSe₂ thin film [26]. The Gibbs free energy changes for the chemical reactions of $2\text{Se} + \text{Mo} = \text{MoSe}_2$ and $2\text{SnSe}_2 + \text{Mo} = 2\text{SnSe} + \text{MoSe}_2$ are calculated by the chemical software of enthalpy, entropy and heat capacity (HSC) 5.0 (Outotec Ltd., Pori, Finland). The Gibbs free energy changes of the two reactions are negative, implying that both of the chemical reactions may occur spontaneously. However, in our previous study [22], the formation of MoSe₂ layer is very slow when the selenization of metal precursor is at a low Se partial pressure atmosphere. Therefore, we can conclude that the formation of the MoSe₂ layer in sample A3 is dominated by the reaction of $2\text{SnSe}_2 + \text{Mo} = 2\text{SnSe} + \text{MoSe}_2$, owing to the excess of SnSe_x from the reactions of $\text{Cu}_x\text{Sn}_y + 2\text{Se}_{x(g)} \rightarrow \text{Cu}_{2-x}\text{Se} + \text{SnSe}_x$ during selenization. The three CZTSe films had very different surface morphologies and cross-sectional images. The CZTSe films that were prepared by sample A1 (very Sn-poor CuSnZn precursor) contained large grains, as presented in Figure 5d with many large gaps or holes at the grain boundaries. From the equilibrium phase diagram, there exists a very small region for the formation of a single phase CZTSe thin film [27]. No Cu-Zn-Se and Sn-Zn-Se ternary phases can form in CZTSe films. In sample A1, the CuSnZn precursor was very Cu-rich and Sn-poor. The ZnSe, Cu_{2-x}Se and CZTSe phases co-existed in the film during the initial annealing process. Cu_{2-x}Se is liquid phase at a temperature of 570 °C, effectively promoting the peritectic reaction and grain growth [28]. However, in sample A3 (very Sn-rich CuSnZn precursor) in Figure 5c,f, the grains are small, and the surface morphology is compact. Many secondary phases are present at the CZTSe/Mo interface. The Cu_{2-x}Se is quickly consumed by the reaction (2) with the

SnSe_x phase to form Cu_2SnSe_3 phase in the initial selenization. The CZTSe thin film is formed by the solid reaction (3), and small grains are therefore obtained.

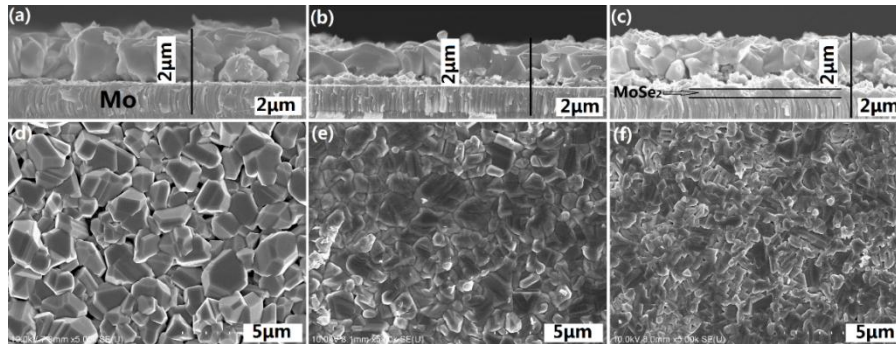


Figure 5. The surface morphology and cross-sectional SEM images of the CZTSe films that were prepared by the selenization of the precursor with samples (a,d) A1; (b,e) A2; and (c,f) A3.

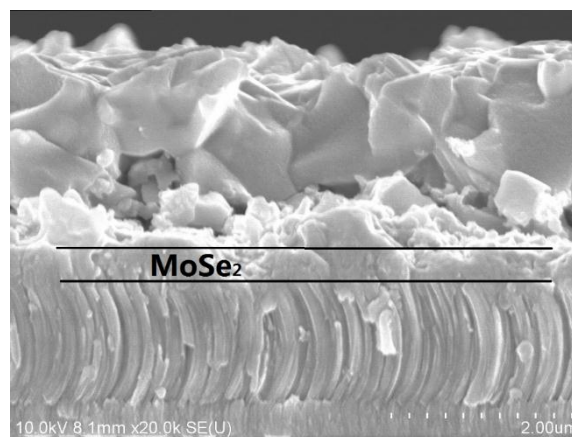


Figure 6. The magnification SEM image of Figure 5c.

Figure 7 presents the two dimensional surface profiles of the CZTSe films that correspond to Figure 5d–f, respectively. The root-mean-square (RMS) roughness for samples A1, A2, and A3 are 245.8, 122.3, and 105.8 nm, respectively. A high rough surface was obtained when the metal precursor was Sn-poor, consistent with the SEM observations in Figure 5. The liquid Cu_{2-x}Se phase promotes grain growth and forms a rough surface during selenization. Figure 8a–c present the line scanning EDS depth profiles of the CZTSe films that correspond to Figure 5a–c, respectively. Figure 8a presents a uniform element distribution of Cu, Sn, Zn, and Se element from surface to the CZTSe/Mo interface. Figure 8b presents weak Sn, Zn, and Se element signals from the CZTSe/Mo interface, corresponding to a thin interface layer of secondary phases. However, in Figure 8c, clear Sn, Zn, and Se element signal are obtained from the CZTSe/Mo interface, corresponding to a thick interface layer that comprises secondary phases. Figure 9 present the SIMS depth profiles of the CZTSe films that were prepared by the selenization of the precursor with samples A1, A2, and A3, consistent with the line scanning EDS observation in Figure 8. The excess signals of Se and Zn elements from the observation of line scanning EDS or SIMS measurement indicate that ZnSe secondary phases possibly exist at the back contact. The secondary phases of ZnSe at the back contact may introduce a high series resistance and degrade

the performance of solar cells [29,30]. The Se signal diffuses deeply into the Mo substrate, indicating that a thick MoSe₂ layer formed at the CZTSe/Mo interface, consistent with the XRD observation in Figure 4b.

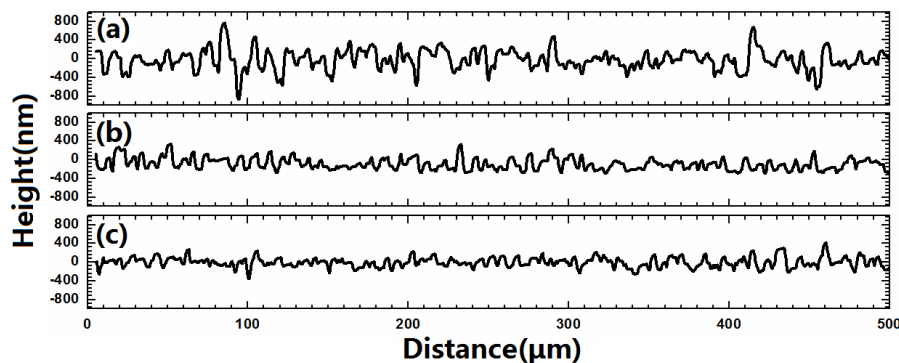


Figure 7. (a–c) present the two dimensional surface profiles of the CZTSe films that correspond to Figure 5d–f, respectively.

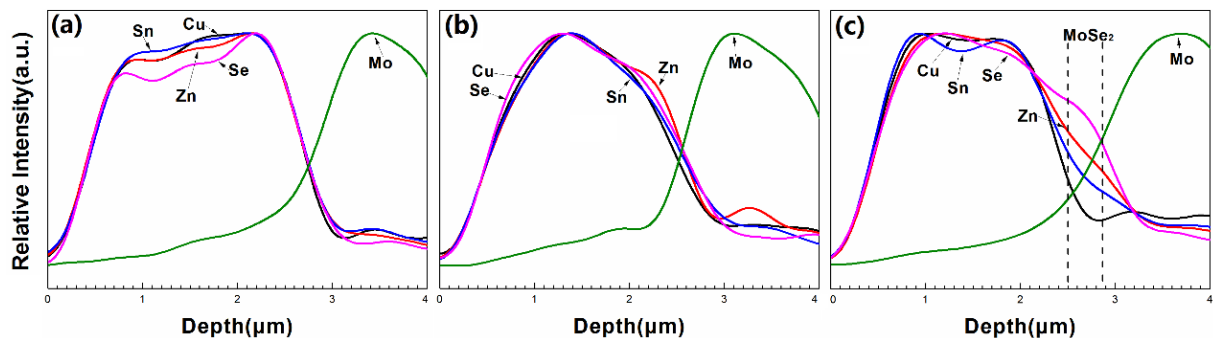


Figure 8. The line scanning energy dispersive spectroscopy (EDS) depth profiles of the CZTSe films that were prepared by the selenization of the precursor with samples (a) A1; (b) A2; and (c) A3.

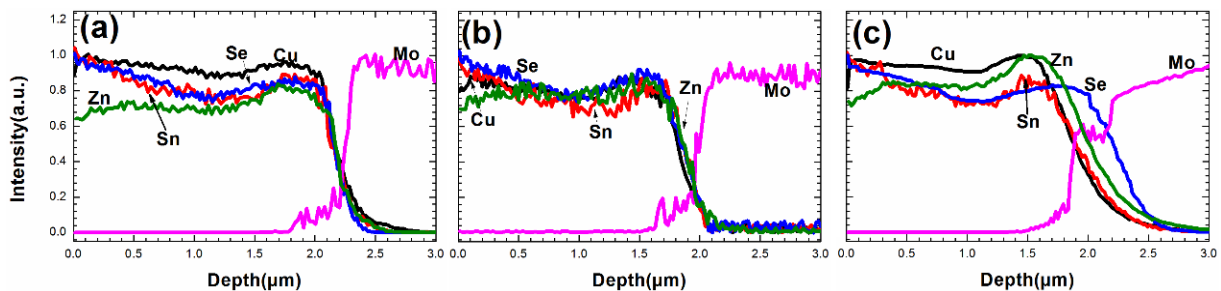


Figure 9. The secondary ion mass spectroscopy (SIMS) depth profiles of the CZTSe films that were prepared by the selenization of the precursor with samples (a) A1; (b) A2; and (c) A3.

Figure 10 plots current-voltage (I-V) curves of three CZTSe solar cells by using films that were formed by the selenization of the precursor with samples A1, A2, and A3 (active area: 0.34 cm²). Table 3 presents the performance parameters of these three solar cells. The CZTSe solar cell that was prepared by using sample A2 exhibited the best device performance with performance parameters of $\eta = 7.94\%$, $V_{oc} = 0.394$ V, $J_{sc} = 34.51$ mA·cm⁻², and $FF = 0.584$. However, the CZTSe solar cell prepared by sample A1 exhibits the worst performance with performance parameters of $\eta = 4.30\%$, $V_{oc} = 0.316$ V, $J_{sc} = 30.59$ mA·cm⁻², and $FF = 0.445$. Large grain boundaries provide a leakage current path, and the rough surface may form many recombination centers at CZTSe/CdS interface [31], seriously degrading

the performance of device that was fabricated by using sample A1. However, small grains and thick MoSe₂ layer at CZTSe/Mo interface may be responsible for the poor performance of sample A3.

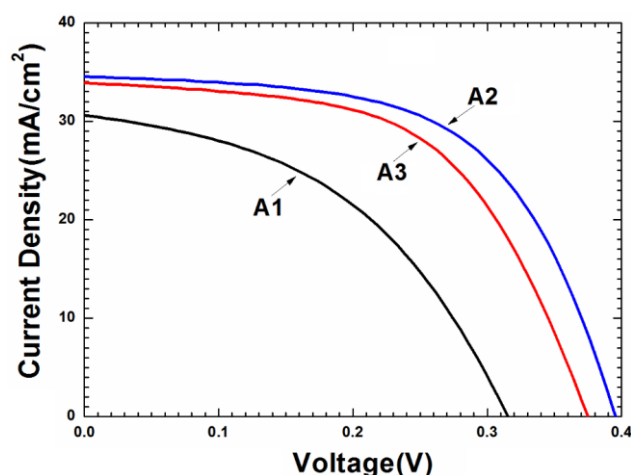


Figure 10. Current-voltage (I-V) curves of three CZTSe solar cells by using films that were formed by the selenization of the precursor with samples A1, A2, and A3.

Table 3. Performance parameters of CZTSe solar cells that were prepared by the precursor samples of A1, A2, and A3.

Sample	Eff (%)	Voc (mV)	Jsc (mA·cm ⁻²)	FF	Rs (Ω)	Rsh (Ω·cm ²)
A1	4.30	316	30.59	0.445	3.1	49
A2	7.94	394	34.51	0.584	2.6	265
A3	7.10	376	33.92	0.557	2.72	112

4. Conclusions

The effect of Sn content of the CuSnZn precursor on the formation of CZTSe films was studied. Experiments revealed that the Sn content of the precursor in the selenization in a low-pressure vapor atmosphere only slightly influences the elemental composition of CZTSe films. However, the Sn content of the precursor significantly affects the grain size and surface morphology of formed CZTSe films. A Sn-poor metal precursor tends to lead to the growth of a CZTSe film with large grains and a rough surface, whereas a Sn-rich precursor tends to lead to the growth of a CZTSe film with small grains and a compact surface. Additionally, the Sn content of the precursor greatly affects the formation of MoSe₂ thin film: A Sn-rich metal precursor leads to the growth of a thicker MoSe₂ thin film than does a Sn-poor precursor, because excess Sn is catalyzing. A CZTSe solar cell with an efficient of 7.94% was realized by using the metal precursor with a Sn/Cu ratio of 0.5 in the selenization process in a low-pressure Se+SnSe_x vapor atmosphere.

Acknowledgments: The authors would like to thank Chang Gung University, Chang Gung Memorial Hospital, and the Ministry of Science and Technology, Republic of China for financially supporting this research under the Contract No. NERP2C0181, BMRPA52, and MOST 102-2221-E-182-041.

Author Contributions: Liyong Yao carried out the electrodeposition of stacked metal layer and selenization, and drafted the manuscript. Jianping Ao carried out the design of electrodeposition and coordination. Ming-Jer Jeng carried out the discussion of experimental results and helped to revise the manuscript. Jinlian Bi carried out the Mo deposition by Sputtering. Shoushuai Gao carried out ZnO and AZO depositions by sputtering. Guozhong Sun carried out the CdS deposition by CBD and the performance measurement of solar cells. Qing He carried out the metallization for solar cells. Zhiqiang Zhou carried out the characterization of CZTSe thin films. Yun Sun participated in the discussion of experimental results and coordination. Liann-Be Chang participated in the discussion of experimental results.

Conflicts of Interest: The authors declare no conflict of interest.

References

1. Ki, W.; Hillhouse, H.W. Earth-abundant element photovoltaics directly from soluble precursors with high yield using a non-toxic solvent. *Adv. Energy Mater.* **2011**, *1*, 732–735. [[CrossRef](#)]
2. Polizzotti, A.; Repins, I.L.; Noufi, R.; Wei, S.-H.; Mitzi, D.B. The state and future prospects of kesterite photovoltaics. *Energy Environ. Sci.* **2013**, *6*, 3171–3182. [[CrossRef](#)]
3. Mitzi, D.B.; Gunawan, O.; Todorov, T.K.; Wang, K.; Guha, S. The path towards a high-performance solution-processed kesterite solar cell. *Sol. Energy Mater. Sol. Cells* **2011**, *95*, 1421–1436. [[CrossRef](#)]
4. Lee, Y.S.; Gershon, T.; Gunawan, O.; Todorov, T.K.; Gokmen, T.; Virgus, Y.; Guha, S. $\text{Cu}_2\text{ZnSnSe}_4$ thin-film solar cells by thermal co-evaporation with 11.6% efficiency and improved minority carrier diffusion length. *Adv. Energy Mater.* **2014**, *5*. [[CrossRef](#)]
5. Wang, W.; Winkler, M.T.; Gunawan, O.; Gokmen, T.; Todorov, T.K.; Zhu, Y.; Mitzi, D.B. Device characteristics of CZTSSe thin-film solar cells with 12.6% efficiency. *Adv. Energy Mater.* **2014**, *4*. [[CrossRef](#)]
6. Haass, S.G.; Diethelm, M.; Werner, M.; Bissig, B.; Romanyuk, Y.E.; Tiwari, A.N. 11.2% efficient solution processed kesterite solar cell with a low voltage deficit. *Adv. Energy Mater.* **2015**, *5*. [[CrossRef](#)]
7. Collord, A.D.; Hillhouse, H.W. The effect of nanocrystal reaction time on $\text{Cu}_2\text{ZnSn}(\text{S},\text{Se})_4$ solar cells from nanocrystal inks. *Sol. Energy Mater. Sol. Cells* **2015**, *141*, 383–390. [[CrossRef](#)]
8. Todorov, T.K.; Tang, J.; Bag, S.; Gunawan, O.; Gokmen, T.; Zhu, Y.; Mitzi, D.B. Beyond 11% efficiency: Characteristics of state-of-the-art $\text{Cu}_2\text{ZnSn}(\text{S},\text{Se})_4$ solar cells. *Adv. Energy Mater.* **2013**, *3*, 34–38. [[CrossRef](#)]
9. Winkler, M.T.; Wang, W.; Gunawan, O.; Hovel, H.J.; Todorov, T.K.; Mitzi, D.B. Optical designs that improve the efficiency of $\text{Cu}_2\text{ZnSn}(\text{S},\text{Se})_4$ solar cells. *Energy Environ. Sci.* **2013**, *7*, 1029–1036. [[CrossRef](#)]
10. Shin, B.; Gunawan, O.; Zhu, Y.; Bojarczuk, N.A.; Chey, S.J.; Guha, S. Thin film solar cell with 8.4% power conversion efficiency using an earth-abundant $\text{Cu}_2\text{ZnSnS}_4$ absorber. *Prog. Photovol. Res. Appl.* **2013**, *21*, 72–76. [[CrossRef](#)]
11. Vauche, L.; Risch, L.; Sánchez, Y.; Dimitrievska, M.; Pasquinelli, M.; Goislard de Monsabert, T.; Grand, P.-P.; Jaime-Ferrer, S.; Saucedo, E. 8.2% pure selenide kesterite thin-film solar cells from large-area electrodeposited precursors. *Prog. Photovol. Res. Appl.* **2016**, *24*, 38–51. [[CrossRef](#)]
12. Ahmed, S.; Reuter, K.B.; Gunawan, O.; Guo, L.; Romankiw, L.T.; Deligianni, H. A high efficiency electrodeposited $\text{Cu}_2\text{ZnSnS}_4$ solar cell. *Adv. Energy Mater.* **2012**, *2*, 253–259. [[CrossRef](#)]
13. Guo, L.; Zhu, Y.; Gunawan, O.; Gokmen, T.; Deline, V.R.; Ahmed, S.; Romankiw, L.T.; Deligianni, H. Electrodeposited $\text{Cu}_2\text{ZnSnSe}_4$ thin film solar cell with 7% power conversion efficiency. *Prog. Photovol. Res. Appl.* **2014**, *22*, 58–68. [[CrossRef](#)]
14. Jiang, F.; Ikeda, S.; Harada, T.; Matsumura, M. Pure sulfide $\text{Cu}_2\text{ZnSnS}_4$ thin film solar cells fabricated by preheating an electrodeposited metallic stack. *Adv. Energy Mater.* **2013**, *4*. [[CrossRef](#)]
15. Shin, B.; Bojarczuk, N.A.; Guha, S. On the kinetics of MoSe_2 interfacial layer formation in chalcogen-based thin film solar cells with a molybdenum back contact. *Appl. Phys. Lett.* **2013**, *102*, 091907. [[CrossRef](#)]
16. Weber, A.; Mainz, R.; Schock, H.W. On the Sn loss from thin films of the material system Cu-Zn-Sn-S in high vacuum. *J. Appl. Phys.* **2010**, *107*, 013516. [[CrossRef](#)]
17. Scragg, J.J.; Ericson, T.; Kubart, T.; Edoff, M.; Platzer-Björkman, C. Chemical insights into the instability of $\text{Cu}_2\text{ZnSnS}_4$ films during annealing. *Chem. Mater.* **2011**, *23*, 4625–4633. [[CrossRef](#)]
18. Redinger, A.; Berg, D.M.; Dale, P.J.; Siebentritt, S. The consequences of kesterite equilibria for efficient solar cells. *J. Am. Chem. Soc.* **2011**, *133*, 3320–3323. [[CrossRef](#)] [[PubMed](#)]
19. Ennaoui, A.; Lux-Steiner, M.; Weber, A.; Abou-Ras, D.; Kotschau, I.; Schock, H.W.; Schurr, R.; Holzing, A.; Jost, S.; Hock, R.; *et al.* $\text{Cu}_2\text{ZnSnS}_4$ thin film solar cells from electroplated precursors: Novel low-cost perspective. *Thin. Solid Films* **2009**, *517*, 2511–2514. [[CrossRef](#)]
20. Scragg, J.J.; Watjen, J.T.; Edoff, M.; Ericson, T.; Kubart, T.; Platzer-Björkman, C. A detrimental reaction at the molybdenum back contact in $\text{Cu}_2\text{ZnSn}(\text{S},\text{Se})_4$ thin-film solar cells. *J. Am. Chem. Soc.* **2012**, *134*, 19330–19333. [[CrossRef](#)] [[PubMed](#)]
21. Chen, S.; Walsh, A.; Gong, X.G.; Wei, S.H. Classification of lattice defects in the kesterite $\text{Cu}_2\text{ZnSnS}_4$ and $\text{Cu}_2\text{ZnSnSe}_4$ earth-abundant solar cell absorbers. *Adv. Mater.* **2013**, *25*, 1522–1539. [[CrossRef](#)] [[PubMed](#)]
22. Yao, L.; Ao, J.; Jeng, M.-J.; Bi, J.; Gao, S.; He, Q.; Zhou, Z.; Sun, G.; Sun, Y.; Chang, L.-B. CZTSe solar cells prepared by electrodeposition of Cu/Sn/Zn stack layer followed by selenization at low Se pressure. *Nanoscale Res. Lett.* **2014**, *9*, 1–11. [[CrossRef](#)] [[PubMed](#)]

23. Fairbrother, A.; Fontané, X.; Izquierdo-Roca, V.; Espíndola-Rodríguez, M.; López-Marino, S.; Placidi, M.; Calvo-Barrio, L.; Pérez-Rodríguez, A.; Saucedo, E. On the formation mechanisms of Zn-rich $\text{Cu}_2\text{ZnSnS}_4$ films prepared by sulfurization of metallic stacks. *Sol. Energy Mater. Sol. Cells* **2013**, *112*, 97–105. [[CrossRef](#)]
24. Beck, M.E.; Swartzlander-Guest, A.; Matson, R.; Keane, J.; Noufi, R. CuIn(Ga)Se₂-based devices via a novel absorber formation process. *Sol. Energy Mater. Sol. Cells* **2000**, *64*, 135–165. [[CrossRef](#)]
25. Yaws, C.L. *Handbook of Vapor Pressure: Volume 4: Inorganic Compounds and Elements*; Gulf Professional Publishing: Houston, TX, USA, 1995; Volume 4.
26. Scragg, J.J.; Dale, P.J.; Colombara, D.; Peter, L.M. Thermodynamic aspects of the synthesis of thin-film materials for solar cells. *ChemPhysChem* **2012**, *13*, 3035–3046. [[CrossRef](#)] [[PubMed](#)]
27. Dudchak, I.V.; Piskach, L.V. Phase equilibria in the Cu_2SnSe_3 - SnSe_2 - ZnSe system. *J. Alloy. Compd.* **2003**, *351*, 145–150. [[CrossRef](#)]
28. Chakrabarti, D.J.; Laughlin, D.E. The Cu-Se (copper-selenium) system. *Bull. Alloy. Phase Diagrams* **1981**, *2*, 305–315. [[CrossRef](#)]
29. Fairbrother, A.; Fontané, X.; Izquierdo-Roca, V.; Placidi, M.; Sylla, D.; Espíndola-Rodríguez, M.; López-Mariño, S.; Pulgarín, F.A.; Vigil-Galán, O.; Pérez-Rodríguez, A.; *et al.* Secondary phase formation in Zn-rich $\text{Cu}_2\text{ZnSnSe}_4$ -based solar cells annealed in low pressure and temperature conditions. *Prog. Photovol. Res. Appl.* **2014**, *22*, 479–487. [[CrossRef](#)]
30. Hsu, W.-C.; Repins, I.; Beall, C.; DeHart, C.; Teeter, G.; To, B.; Yang, Y.; Noufi, R. The effect of Zn excess on kesterite solar cells. *Sol. Energy Mater. Sol. Cells* **2013**, *113*, 160–164. [[CrossRef](#)]
31. Wang, K.; Gunawan, O.; Todorov, T.; Shin, B.; Chey, S.J.; Bojarczuk, N.A.; Mitzi, D.; Guha, S. Thermally evaporated $\text{Cu}_2\text{ZnSnS}_4$ solar cells. *Appl. Phys. Lett.* **2010**, *97*, 143508. [[CrossRef](#)]



© 2016 by the authors; licensee MDPI, Basel, Switzerland. This article is an open access article distributed under the terms and conditions of the Creative Commons by Attribution (CC-BY) license (<http://creativecommons.org/licenses/by/4.0/>).